

Link prediction with swarms of chiral quantum walks

Gaia Forghieri,^{1,*} Viacheslav Dubovitskii,² Matteo A. C. Rossi,² and Matteo G. A. Paris¹

¹*Dipartimento di Fisica, Università di Milano, I-20133 Milan, Italy*

²*Algorithmiq Ltd., Kanavakatu 3 C, FI-00160 Helsinki, Finland*

(Dated: November 19, 2025)

Reconstructing protein–protein interaction networks is a central challenge in network medicine, often addressed using link prediction algorithms. Recent studies suggest that quantum walk-based approaches hold promise for this task. In this paper, we build on these algorithms by introducing chirality through the addition of random phases in the Hamiltonian generators. The resulting additional degrees of freedom enable a more diverse exploration of the network, which we exploit by employing a swarm of chiral quantum walks. Thus, we enhance the predictive power of quantum walks on complex networks. Indeed, compared to a non-chiral algorithm, the chiral version exhibits greater robustness, making its performance less dependent on the optimal evolution time—a critical hyperparameter of the non-chiral model. This improvement arises from complementary dynamics introduced by chirality within the swarm. By analyzing multiple phase-sampling strategies, we identify configurations that achieve a practical trade-off: retaining the high predictive accuracy of the non-chiral algorithm at its optimal time while gaining the robustness typical of chirality. Our findings highlight the versatility of chiral quantum walks and their potential to outperform both classical and non-chiral quantum methods in realistic scenarios, including comparisons between successive versions of evolving databases.

I. INTRODUCTION

Link prediction is a fundamental problem in network science, with applications on network reconstruction spanning from friendship recommendations in social media [1–3] to biological systems [4–7]. In regards to the latter, protein-protein interaction (PPI) networks, also called *interactomes*, constitute a challenge of critical importance. Indeed, these networks map all known interactions between proteins occurring within the cell of an organism [8–12]. Therefore, they are crucial in understanding cellular processes and disease mechanisms [13–15], ultimately enabling optimal drug design [16–18]. However, the currently available data on experimentally validated interactions is still largely incomplete, with human interactome databases estimated to cover only a small fraction

* gaia.forghieri@unimi.it

of the whole structure ($\lesssim 10\%$) [11, 19, 20].

Due to the great sparsity and incompleteness of PPI networks, a great deal of link prediction methods have been tested on them [4, 21–23]. In this context, accurate link prediction is essential, since it provides a basis for guiding experimental validation with an efficient selection of candidate links that are most likely to exist. Among the possible methods, those based on continuous-time random walks (RW's) have proven to be particularly effective [24–27]. Indeed, the evolution of a walker along the network explores its whole topology, potentially predicting links between far-distant nodes.

Recent works have extended the RW-based method to its quantum counterpart, introducing continuous-time quantum walks (QWs) [28–30]. Thanks to its quantum nature, the QW allows for phenomena that are classically absent, most notably superposition and interference between different trajectories of the walker. Consequently, the evolution of a QW is drastically different from that of the RW and, under the appropriate conditions, can be faster and even reach the ballistic regime [31–35]. This has proven to greatly improve the efficiency in the exploration of the network topology, consequently enhancing the performance for link prediction. Additionally, the same formalism can be adopted for many other problems in the scope of network science, such as disease gene prioritization [36, 37], and more.

That said, QW-based link prediction methods up to now have relied on symmetric, real-valued Hamiltonians directly derived from the adjacency or Laplacian matrices of the graph. However, this is an unnecessary restriction. Instead, a more general Hamiltonian generator can be built through the introduction of complex phases for each edge of the network. In this context, we talk about *chiral* QW's [38–40], since these phases induce a directional bias in the evolution of the walker. This property can dramatically alter transport properties on graphs, and is consequently a key ingredient in enhancing QW-based algorithms, such as quantum transport [40–45], state transfer [46–49], and so on.

In this paper, we study the effects of chirality on the link prediction problem, by exploiting the wide range of dynamics offered by the phases as new degrees of freedom. Specifically, we combine multiple QW's with different directional biases, to form what we call a *swarm* of chiral QW's. In this way, we aim at enhancing the exploration of sparse and irregular networks, possibly complementing the non-chiral evolution. We compare the chiral and non-chiral performances on multiple real-world PPI networks, and demonstrate in which regimes the use of chirality allows to outperform the non-chiral method.

Our results demonstrate that chiral quantum walks may significantly enhance link prediction

performance, particularly in largely incomplete PPI networks. By combining multiple chiral walks into a swarm, we introduce complementary dynamics that bring an improved stability of the performance over time and, under certain conditions, even outperform the non-chiral performance at the optimal time. These findings suggest that chirality is a powerful tool for overcoming the limitations of conventional quantum walks in reconstructing interactomes, often complementing other best known methods from literature.

The paper is organized as follows: Section II introduces the theoretical framework for chiral quantum walks and the metrics used for link prediction. Section III presents our results, beginning with a preliminary analysis on the behavior of swarms of chiral QW's in comparison to a single non-chiral QW, both at reference unitary time and in terms of dynamics. We then compare our method to other approaches from literature and analyze its efficacy across diverse PPI networks. At the end, we briefly focus on link prediction applied on the comparison of different temporal versions of the same network, to better assess the performance on real-case scenarios. Finally, Section IV discusses implications and future directions, while Appendices provide additional technical details on dynamical distances between walker evolutions and performance metrics.

II. METHODS

We consider complex networks modeled by unweighted and undirected graphs $G(V, E)$, with V the set of nodes of size n and E the set of edges. The adjacency matrix of G is defined as an $n \times n$ matrix:

$$A = (A_{jk}) = \begin{cases} 1 & \text{if } (j, k) \in E, \\ 0 & \text{if } (j, k) \notin E. \end{cases} \quad (1)$$

Another important definition is the degree of node j , $d_j = \sum_k A_{jk}$, defined as the number of links emanating from node j .

A. Continuous-time quantum walks

The description of the QW requires the definition of an n -dimensional Hilbert space \mathcal{H} . Each vector of its orthonormal basis $\{|j\rangle\}_{j=1}^n$ represents a state completely localized on node i of G . Within this formalism, the occupation probability of each node at time t is $p_j(t) = |\langle j|\psi(t)\rangle|^2$, where $|\psi(t)\rangle$ is a generic quantum state in \mathcal{H} . The QW evolution is described by the Schrödinger

equation:

$$|\psi(t)\rangle = \mathcal{U}(t) |\psi(0)\rangle, \quad (2)$$

where $|\psi(0)\rangle$ is the initial state of the system, and $\mathcal{U}(t) = e^{-iHt}$ is the unitary evolution operator (fixing $\hbar = 1$). Thus, the transition probability from nodes j to k reads $P_{jk}(t) = |\langle j | \mathcal{U}(t) | k \rangle|^2$.

The only conditions in choosing the Hamiltonian generator H for the evolution of the system are for it to be Hermitian, so that \mathcal{U} is unitary, and compatible with the network's topology. Consequently, a possible choice is to directly associate $H \equiv A$. However, one can generalize the concept to include complex phases on the off-diagonal elements of A :

$$\mathcal{H}_\phi = (\mathcal{H}_{\phi,jk}) = \begin{cases} e^{i\phi_{jk}} & \text{if } (j, k) \in E, \\ 0 & \text{if } (j, k) \notin E, \end{cases} \quad (3)$$

with $\phi_{kj} = -\phi_{jk}$. These phases can be interpreted as the action of gauge fields acting on the system [50–52]. Since these introduce a directional bias in the dynamics of the walker, we talk in this case of a *chiral* quantum walk (c-QW) [38]. The special case in which all phases are zero now takes the name of *non-chiral* quantum walk (nc-QW). One can immediately notice how the introduction of such phases implies the existence of infinitely many c-QW's for each nc-QW. This opens up the possibility to explore a much wider range of dynamics, and consequently optimize the quantum advantage for the task of interest [40].

B. Metrics for link prediction

The objective of link prediction is to infer the missing links in G based on the known structure of G . Therefore, a link prediction algorithm usually consists of a scoring scheme that produces a ranking of all possible pairs of non-connected nodes in G . Ideally, the higher the score of the pair is, the higher the probability that a link is present in the unknown structure of G . Link prediction methods that involve the evolution of a nc-QW on complex networks have already been studied [28–30], and typically evaluate the score of each non-connected pair (j, k) as a function of the transition probability between nodes j and k after an evolution of time t . Indeed, these methods rely on the intuition that a link is more likely to occur between two nodes if the walker is more likely to move from one to the other. We will refer to the scoring system defined previously by Goldsmith et al. [29]:

$$S(j, k; t) = P_{jk}(t)(d_j + d_k), \quad (4)$$

for $j \neq k$, which also takes into account the degree of the nodes involved, as high-degree nodes are the most likely to be connected to other nodes.

As we can consider multiple QW's evolving on G , we can imagine that each will explore the network differently, and potentially predict missing links in areas that are unexplored by the others. This is a direct consequence of the directionality imposed on the walker dynamics by the chiral phases in the Hamiltonian from Eq. (3). Because of this, a possible strategy to try and maximize the performance of link prediction is to exploit a *swarm* of quantum walks, and keep for each non-connected pair the maximum score predicted by each QW. We can thus define, for M chiral walkers, an overall chiral score:

$$S_c^M(j, k; t) = \max(\{S_m(j, k; t)\}_{m=1}^M), \quad (5)$$

where $S_m(j, k; t)$ is the score obtained by the m -th c-QW. In the same way, one can combine results from both the non-chiral and chiral cases, obtaining a total score of:

$$S_{tot}^M(j, k; t) = \max(S_{nc}(j, k; t), S_c^M(j, k; t)), \quad (6)$$

where $S_{nc}(j, k; t)$ is the score from the nc-QW.

The whole structure of PPI networks is generally unknown. Therefore, we test the performance of our link prediction algorithm on a certain dataset by assessing its capability to retrieve a fraction of randomly removed links using the remaining information on the dataset. That is to say, for each considered network we randomly remove $N\%$ of the existing links. All removed links are considered positive test cases, while the non-edges from the original dataset are negative test cases. Subsequently, we run our prediction algorithm on the remaining structure of the graph. All the non-edges are ranked in descending order according to the scores from Eqs. (4-6): the higher the score, the more likely is the link to exist. Finally, the edges whose score is higher than a certain cut-off threshold are considered positive predictions, while all the other edges are negative predictions.

This approach allows us to define the following metrics for each value of the threshold:

$$\text{precision} = \frac{\text{TP}}{\text{TP} + \text{FP}}; \quad \text{recall} = \text{TPR} = \frac{\text{TP}}{\text{TP} + \text{FN}}; \quad \text{FPR} = \frac{\text{FP}}{\text{FP} + \text{TN}}; \quad (7)$$

where TP = true positives, FP = false positives, TN = true negatives, FN = false negatives. TPR/FPR stand for true/false positive rate, respectively. The figures of merit we will refer to in Sec. III are the area under the receiver-operator characteristic curve (AuROC, TPR vs. FPR) and the area under the precision-recall curve (AuPR, precision vs. recall). Both of these metrics have

been extensively used in link prediction and more general binary classification problems. Of the two, the AuROC is the more extensively used in literature, thanks to its easier interpretability [53]. Indeed, it can be interpreted as the probability of correctly predicting a link chosen at random from the positive set, over a wrong link chosen at random from the negative set. On the other hand, the AuPR focuses only on the positive class, and is consequently the more relevant for scenarios where the ratio between positive and negative cases is extremely small. This is the case for PPI networks, which generally present high sparsity. Additionally, it is the more suited for evaluating early retrieval performance, an extremely important aspect for biological applications [54].

III. RESULTS

In our study, we considered five different networks. Three of them are from the HINT database [9], version 2024-6: *Musculus*-HINT, corresponding to the common house mouse; *Yeast*-HINT, i.e., the *Saccharomyces Cerevisiae* yeast commonly used for baking; and *Human*-HINT. We also use the *Yeast*-BioGRID network, still for *S. Cerevisiae*, from the BioGRID database [55], version 4.4.248, compiled on July 25th, 2025, to compare results on the same organism from different databases. For the same reason, we also include the Human Protein Reference Database (HPRD) from its latest update [56]. For each of these networks, we consider only the largest component. Additionally, we don't consider self-edges, since these have little to no influence on the performance [29], and are not modified by the introduction of chiral phases. Some statistics of the resulting networks are reported in Table I, and represented graphically in Fig. 1.

Network	$ V $	$ E $	$\langle k \rangle$	ρ	C
Musculus - HINT	1,486	2,423	3.261	0.0022	0.108
Yeast - HINT	5,438	28,319	10.415	0.0019	0.148
Yeast - BioGRID	5,892	34,418	11.683	0.0020	0.119
Human - HPRD	8,498	33,935	7.987	0.0009	0.109
Human - HINT	11,319	38,332	6.773	0.0006	0.205

TABLE I. Some properties of the networks that were tested. $|V|$: number of nodes, $|E|$: number of edges (excluding self-edges), $\langle k \rangle$: average degree, ρ : network density, C : average clustering coefficient.

In the following, we study the k -fold cross-validation for 10% ($k = 10$), 20% ($k = 5$) and 50% ($k = 2$) link removal. We repeat the cross-validation $r = 2$ times for 20% and $r = 5$ times for 20%, in order to average the results on a total of 10 trials for each case. Firstly, in Sec. III A, we compare the performances of nc-QW's and c-QW's on *Musculus*-HINT, the smallest network

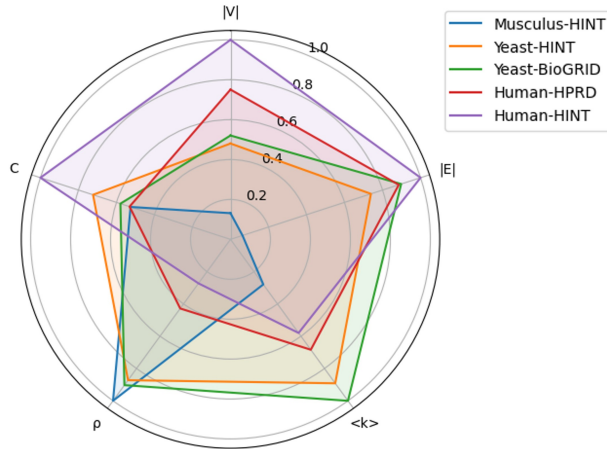


FIG. 1. Radar chart of normalized metrics for each network from Table I. Each quantity $q \in \{|V|, |E|, \langle k \rangle, \rho, C, A\}$ is normalized through the equation $q^{\text{Norm}} = q/q^{\text{max}}$, where the maximum is evaluated among all considered networks.

considered in this work (see Table I), to get a general idea on how to efficiently build a link prediction algorithm based on chirality. Here, in Sec. III A 1 we first focus on how to better exploit multiple complementary c-QW's at a reference unitary time. We then analyse the dynamical behaviour of the performance in Sec. III A 2. Finally, in Sec. III B we study the performance on multiple PPI networks, comparing our QW-based algorithms with other well-known approaches from literature, with an additional focus on version comparison in Sec. III B 1.

A. Swarm performance

1. Making the most of chiral complementarity

We start our analysis by considering the effects of the contribution of multiple c-QW's to our algorithm, which we refer to as a *swarm* of chiral walkers. We consider t as a hyperparameter of our problem, on which the performance can be optimized. However, understanding the optimal value of t requires *a priori* knowledge on the evolution of the performance, something which in general varies wildly depending on the graph structure and is not usually known in real-life scenarios. For this reason, in this first section we fix $t = 1$, a value that is generally close to the optimal time interval (see the later analysis in Sec. III A 2), and that can be taken as a reference for one-shot experiments.

In Fig. 2(a) we show the number of true positive predictions at each threshold with only chiral

contributions to the score [see Eq. (5)]. These trials were performed at 10% link removal for the smallest network we considered in our study, i.e. Musculus-HINT (see Table I). We considered an increasing number of c-QW's with phases sampled randomly in the interval $\phi_{jk} \in [-\pi, \pi]$. These results show that the early retrieval rate of the link prediction algorithm steadily increases with the number of considered c-QW's. This behaviour can be explained by the possibility of exploring a wider range of dynamics thanks to the directionality introduced by the chiral phases. Indeed, due to the highly complex structure of the considered network, the evolution of a single walker may concentrate on specific areas of the graph, and consequently miss the presence of potential links in other regions. Instead, a second walker with different chirality may potentially explore the graph differently, and consequently recover information that the first walker missed. Eventually, a swarm of a sufficient number of walkers is likely to explore the complete structure of the graph, thus saturating the performance, as seen in Fig. 2(a) for ~ 10 c-QW's.

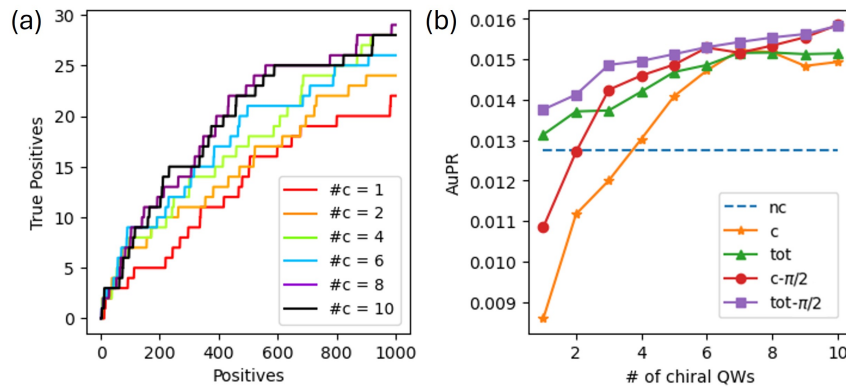


FIG. 2. Performance of link prediction at 10% link removal on the Musculus-HINT network as a function of the number of considered chiral QW's, at fixed $t = 1$. Panel (a) shows the number of links correctly predicted (true positives) among the first predicted non-edges with highest score (positives) for a single fold, considering an increasing number of c-QW's with random phases and without the nc-QW's contribution. Panel (b) shows the convergence of the average AuPR from 10-fold cross-validation. The label 'nc' stands for non-chiral; 'c' and 'tot' refer to the chiral case with random phases, respectively with and without the contribution from the nc-QW; the suffix ' $\pi/2$ ' is used to differentiate the case with phases sampled as random multiples of $\pi/2$ rather than from the continuous interval $[-\pi, \pi]$ (with no suffix).

We then show in Fig. 2(b) the average AuPR from the 10-fold cross-validation on the same network. In this picture, we show results obtained from evaluating the score either with chiral contributions alone [Eq. (5)], or by including the non-chiral case as well [Eq. (6)]. The reported curves confirm our previous considerations. Indeed, in both cases the AuPR increases as a function

of the number of c-QW's making up the swarm, until it mostly converges for ~ 10 c-QW's. Most importantly, for a high enough number of walkers, the performance can potentially exceed that of the nc-QW alone, while a single c-QW on average behaves worse than its non-chiral equivalent. This implies that the power of random chirality stands in the possibility of combining multiple dynamics, while the nc-QW is generally the best choice when using a single walker on its own. Additionally, we show that the inclusion of the nc-QW significantly affects the performance by increasing the AuPR at each step. This confirms that the non-chiral evolution has a particular importance in the exploration of the graph. Indeed, the absence of directionality in the Hamiltonian generator makes it so that the nc-QW already explores in a relatively uniform manner all regions of the graph. The same observations are also valid for the AuROC, though to a lesser extent (see Appendix A).

After these considerations, we introduced a second sampling method for the phases in Eq. (3). This consists in only sampling multiples of $\pi/2$, and rearranging them so that the sum of the phases on each row of H_ϕ is as close to 0 as possible. This choice ensures a set of c-QW's making up the swarm with evolutions that are, on average, as different as possible from the nc-QW and from one another (see Appendix B). In other words, this second sampling method (suffix ' $\pi/2$ ') ensures a more efficient exploration of the configuration space made available by chirality. Consequently, as the AuPR shows, this method consistently enhances the performance, both with and without the non-chiral contribution.

Overall, the results from Fig. 2 show that the nc-QW is the one that, on its own, best explores the graph for link prediction purposes. However, a swarm of c-QW's can match, and sometimes improve, the performance of the nc-QW alone. Specifically, chiral swarms that introduce the largest variety with respect to the non-chiral evolution bring the best performance overall, at least when considering $t = 1$ as a reference time. The next question is whether or not this behaviour is consistent during the whole evolution.

2. Dependence on time

As mentioned above, the problem of maximizing the AuPR requires an optimization on the hyperparameter t , which defines the evolution time of the walkers. In Fig. 3 we show the dependency of the AuPR on time for Musculus-HINT at various link removal rates. For this analysis, we consider the second sampling method from Sec. III A 1 (suffix ' $\pi/2$ '), which we showed to be the more efficient in creating c-QW's with complementary evolutions. We also introduce a new

method (suffix ‘ $\pi/8$ ’), which samples the phases from a small continuous interval, i.e. $[-\pi/8, \pi/8]$. Similarly to the first method from Sec. III A 1, the phases from the $\pi/8$ -method can be any real number in the interval, but now they act as a perturbation on the non-chiral evolution.

Figure 3 shows that, for all percentages of link removal, the walkers require an initial transient time to leave the starting node and adequately explore the surrounding region. During this time, the AuPR increases rapidly, until it reaches a maximum at $t \lesssim 1$. At this point, we can imagine that the walkers have explored most of the topology of the graph. Afterwards, the AuPR starts decreasing, likely due to an overabundance of interference that disrupts the coherence of the quantum walk in its later stages. Eventually, the system reaches a saturation regime, with AuPR values that are significantly lower than those at the maximum.

At the optimal time and for low link removal rates (10% and 20%), the AuPR obtained with the $\pi/2$ -sampling method is below those of the nc-QW or the $\pi/8$ -method. The latter is instead capable of maintaining the non-chiral performance thanks to its perturbative nature. Instead, for high link removal rates (50%) the $\pi/2$ -method largely surpasses the others. Particularly, we observe an increase of $\sim 5.9\%$ for the $\pi/8$ -method and $\sim 8.6\%$ for the $\pi/2$ -method with respect to the maximum of the non-chiral curve. This proves that the best usage of the swarm of c-QW’s is in particularly incomplete networks, such as PPI networks [11, 19, 20]. That said, at all link removal percentages either chiral methods improve the performance at later times ($t \gtrsim 1$). Consequently,

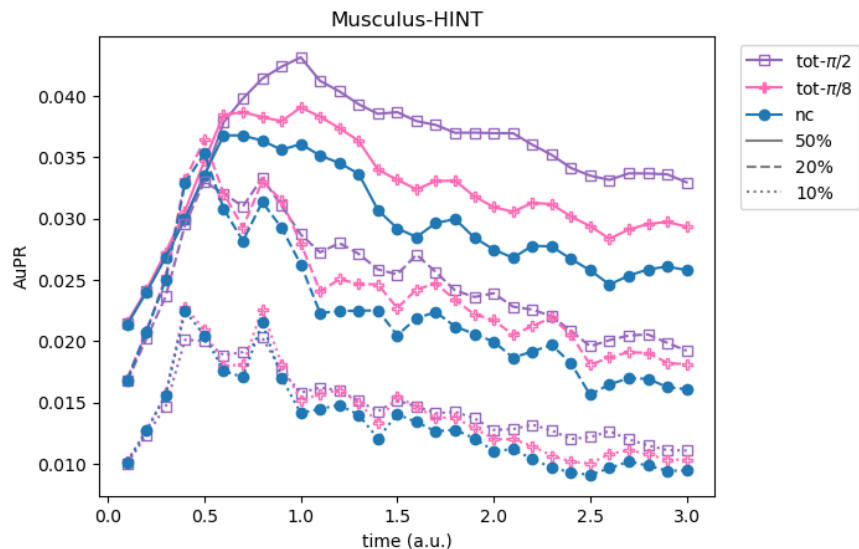


FIG. 3. Evolution in time of the average AuPR on Musculus-HINT obtained through k -fold cross-validation for 10%, 20% and 50% link removal, as explained in the text. Labels follow the same nomenclature as Fig. 2; in addition, the suffix ‘ $\pi/8$ ’ indicates the case with phases sampled from the continuous interval $[-\pi/8, \pi/8]$.

in all cases the chiral swarm provides a more stable performance over time, and thus becomes the most viable option in real-life scenarios in which time optimization is not possible. The $\pi/2$ -method particularly so, due to the walkers' complementarity in evolution, mentioned previously in Sec. III A 1.

Overall, we saw that sampling phases from a smaller interval around 0 provides a much more similar performance to the non-chiral case, thus maintaining its maximal performance in all cases. However, the $\pi/2$ -method provides a much more stable performance over time, especially for high link removal rates. Consequently, the choice over nc-QW's versus c-QW's, and over which sampling method to use, depends mainly on the intended use of the algorithm: specifically, on whether a time optimization is possible, or one-shot measurements at an arbitrary time are required. Despite not reaching the same stability as the $\pi/2$ -method, the $\pi/8$ -method seems to be a good trade-off between the two other options.

B. Application on PPI networks

We then checked the performance of our algorithms on different and larger networks (see Table I), comparing our results with various other methods from literature. Among these, $L3$ was specifically designed to work on PPI networks, and is based on the weighted counting of paths of length three between nodes [4]. *Preferential attachment* (PA) instead evaluates the score as the product of the degree of the nodes [57]. Then, *common neighbour* (CN) analyses the number of neighbours shared by the nodes [58]. *Adamic Adar* (AA) is similar to CN, but adds additional weight to less-connected neighbours [1]. Finally, the *structural perturbation method* (SPM) estimates the predictability on the adjacency matrix of the graph by adding perturbations to it [59]. For the latter we fixed $p^H = 0.1$ and averaged results over 10 runs as in Ref. [59].

In Figs. 5 and 4 we report respectively the AuPR and AuROC for all cases. Notice that we only report on the AuPR at optimal times, to better understand in which cases the maximal performance can be improved with chirality. Otherwise, the same considerations as in Sec. III A stand for all other networks as well, and the $\pi/2$ -method is the one that provides the most stable performance, and the higher AuPR at the reference time of $t = 1$ (not shown). As for the AuROC, its time dependence is negligible and does not affect the ordering of the performances between the QW-methods, so that we directly plot the results at $t = 1$.

The curves of the AuPR in Fig. 4 show good performance for the QW-methods with respect to the other most common algorithms from literature. Specifically, the only two other methods that

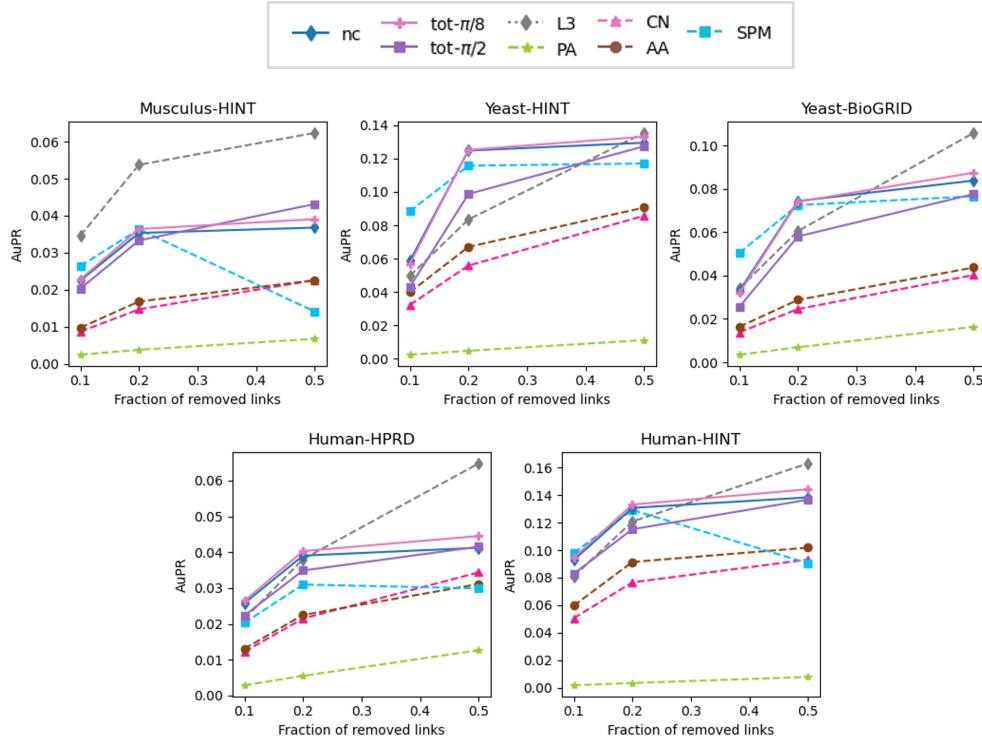


FIG. 4. Average AuPR as a function of the fraction of removed links, obtained through repeated k -fold cross-validation, as explained in the text. All continuous lines refer to our link prediction algorithm using chiral and non-chiral QW's, while all dashed lines correspond to various other methods from literature. Labels follow the same nomenclature as previous Figures.

prove to be always competitive with them are SPM and L3. Both of these are particularly efficient in PPI networks. Indeed, the perturbative nature of the former is effective in predicting missing parts of networks [59], while the latter was specifically designed to capture the basic principles that drive protein interactions [4]. That said, in all cases the QW-algorithms are able to match or even outperform at least one between L3 and SPM, if not both (e.g. Yeast-HINT at 20% link removal).

That said, for all the studied networks, the previous considerations from Sec. III A 2 on the behavior of the QW-methods' optimal AuPR are confirmed apart for one exception. That is, at 50% link removal, the $\pi/2$ -method only outperforms the others in Musculus-HINT, while in all other networks it is hardly able to match the non-chiral performance. Notice that the Musculus network is the denser one and with the lowest clustering coefficient (see Table I). Consequently, this suggests that chirality is less efficient on those networks that, instead, are globally sparser but locally denser, as is the case for the two Yeast networks and the two Human ones.

On the other hand, the $\pi/8$ -method always shows a slight but definite improvement at high link removal rates with respect to the non-chiral method, while still matching it at lower rates. This

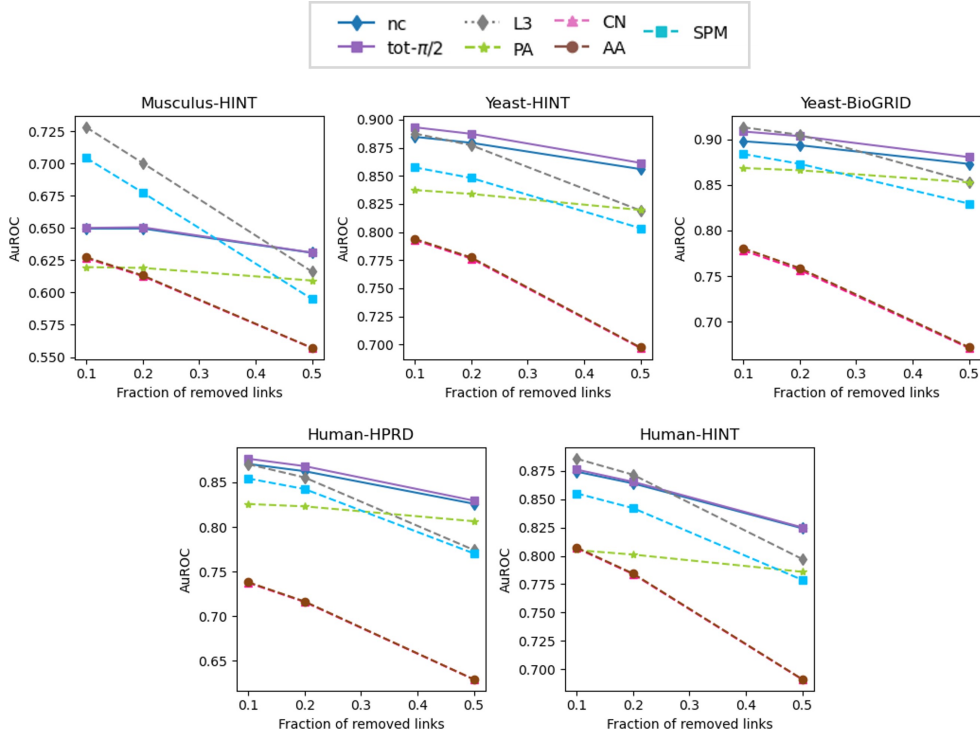


FIG. 5. Average AuROC as a function of the fraction of removed links, obtained through repeated k -fold cross-validation, as explained in the text. All continuous lines refer to our link prediction algorithm using chiral and non-chiral QW's, while all dashed lines correspond to various other methods from literature. Labels follow the same nomenclature as previous Figures.

is because the $\pi/8$ -method is, as mentioned previously, a perturbation on the non-chiral method. Consequently, though still maintaining the same flexibility of a chiral algorithm, each c-QW has an evolution that is more similar to the non-chiral one. Specifically, the $\pi/8$ -method improves the AuPR by 2.8% and 4.3% respectively for Yeast-HINT and Yeast-BioGRID at 50% link removal; and by 8.0% and 4.3% respectively for Human-HPRD and Human-HINT at 50% link removal.

As for the AuROC, Fig. 5 shows that, in almost all cases, the QW-algorithms match/outperform the other best method from literature, i.e. L3. The only striking exception is the Musculus-HINT network at low link removal rate. However, even in this network, the QW-method shows the overall best performance at 50% link removal. This behavior confirms that, as mentioned previously in Sec. 3, the QW-method with either the nc-QW or the swarm of c-QW's is best used when the percentage of missing links is high, as is the case for current PPI databases in general [11, 19, 20]. Additionally, the chiral $\pi/2$ -method always increases, though often very slightly, the non-chiral performance. The $\pi/8$ -method (not shown) is instead always in between the non-chiral performance and the chiral one with the $\pi/2$ -method, thus confirming its nature as a middle-ground between the two other

	Yeast-HINT	Yeast-BioGRID	Human-HINT
CN	0.0138	–	0.279
SPM	0.0352	0.0186	0.233
AA	0.0112	–	0.276
L3	0.0125	–	0.251
PA	–	–	0.0791
Non-chiral	0.0706	0.0170	0.219
Chiral- $\pi/2$	0.0250	0.0285	0.120
Chiral- $\pi/8$	0.0726	0.0120	0.212

TABLE II. AP@ k obtained through the comparison of different versions of the Yeast-HINT, Yeast-BioGRID and Human-HINT databases, for $k = 100$. The times of the QW evolutions were fixed to values close to the optimal times considered for Fig. 4, i.e. $t = 0.3$ for Yeast-HINT; $t = 0.2$ for Yeast-BioGRID; and $t = 0.4$ for Human-HINT. No performance is reported in those cases where no links were found in the first k predictions; the best performance for each column is highlighted in bold. The suffixes of the chiral methods follow the nomenclature used throughout the paper.

methods. The most relevant enhancements are observed in the Yeast-HINT network (0.96% at 10% link removal rate) and in the Yeast-BioGRID network (1.19% at 10% link removal rate).

1. Version comparison

Up to now, we have evaluated the link prediction performance through k -fold cross-validation on specific versions of network databases. That said, an additional benchmark consists of comparing different versions of the same databases, by applying link prediction to earlier versions of the networks studied in this paper. In order to do this, we considered the versions of the Yeast-HINT, Yeast-BioGRID and Human-HINT databases previously studied in Ref. [29]. This strategy has low statistical significance, since it relies on a single way in which the databases historically evolved. However, it provides a more realistic assessment of the performance of our algorithms on real-world scenarios, and helps identify which algorithms are more robust to structural changes over time.

Here we evaluate the performance on version comparison through the average precision at k (AP@ k), computed as:

$$\text{AP@}k = \frac{1}{r_k} \sum_{i=1}^k \frac{r_i}{i} \cdot \text{rel}(i), \quad (8)$$

where r_k (r_i) is the number of relevant items, i.e. of correctly predicted links, in the top k (i) predictions; the ratio r_k/k is also called precision at k (P@ k); and $\text{rel}(i)$ is an indicator function

equal to 1 if the item of rank i is relevant, and 0 otherwise. The $AP@k$ measures how well a model ranks the true future links among its top k predictions, reflecting both the accuracy and the relevance of the predicted links. This is especially useful in temporal evaluations, where the goal is to predict the links that actually formed in a newer version of the network. Additionally, by focusing on the top k predictions, the $AP@k$ aligns with real-world scenarios where only a limited number of high-confidence predictions are possible to test, as is the case in PPI network reconstruction.

Table II reports the $AP@k$ for the three networks under consideration and for all the algorithms previously introduced, considering $k = 100$. In both Yeast databases, the best performance corresponds to one of the two chiral methods. Specifically, the increase with respect to the non-chiral one is relatively small for Yeast-HINT with the $\pi/8$ -method ($\sim 2.8\%$), but it is especially high on Yeast-BioGRID with the $\pi/2$ -method ($\sim 67\%$). In these two networks, all QW-based algorithms are particularly better than L3, which consistently outperformed all other methods at high link removal rate in the results from Fig. 4. That is to say that, although L3 performs the best on cross-validation on a single version of a database, it does not necessarily imply the best performance in a real-life scenario. That said, the results from the Human-HINT database show that, in this network, the performance from all methods is much higher than in the Yeast networks. Especially CN, which instead was performing very poorly in Figs. 4 and 5. Here, though the QW performance is slightly lower, it is still in the same order of magnitude as the others.

Overall, considering the values of the $AP@k$ in absolute terms, chirality does not appear to offer a substantial advantage in scenarios where other methods already achieve high performance. However, it proves to be particularly valuable in enhancing the non-chiral method in cases where most other approaches fall short, highlighting its role as a complementary asset within the broader landscape of link prediction techniques.

IV. CONCLUSIONS

In this paper we have generalized a quantum-based approach to link prediction in complex networks, through the use of swarms of chiral quantum walks. Thanks to randomly-sampled complex phases in the Hamiltonian generator, each walker of the swarm possesses a different directional bias that complements the others in the exploration of the networks. While a single non-chiral quantum walk typically outperforms an individual chiral walk due to its uniform exploration, a well-constructed swarm of chiral walkers can explore the network more thoroughly and stably

over time. This advantage becomes particularly relevant in real-world scenarios where the optimal evolution time is unknown. By employing targeted phase sampling strategies—such as maximizing dynamical diversity—chiral swarms achieve greater robustness, sometimes outperforming the non-chiral case at optimal time. When the latter case does not occur, small chiral perturbations offer a practical compromise, preserving the strengths of the non-chiral evolution while enhancing stability over the evolution time.

We then tested our methods across multiple real-world PPI networks, showing that the QW-based algorithms consistently matched or outperformed classical algorithms such as L3 and SPM, particularly in correspondence of high link removal rates. Maximizing the distance between each walker proved most effective in sparse and low-clustering networks. Instead, small perturbations of the non-chiral evolution offered a reliable compromise in more locally dense topologies, notably improving the AuPR by up to 8.0% in the Human-HPRD database. Furthermore, in version comparison experiments—where predictions were made on future links from older network snapshots—chiral methods showed superior performance especially when most other methods failed at retrieving any link in the top 100. These results highlight the complementary role of chirality in enhancing link prediction, particularly in dynamic and largely incomplete network scenarios.

ACKNOWLEDGMENTS

This work has been partially supported by EU (Next Generation Europe) and MUR through the project QWEST-CUPG53D23006270001.

Appendix A: Convergence of AuROC

Figure 6 shows the AuROC at 10% link removal at unitary time from the 10-fold cross-validation on the Musculus-HINT network, as a function of the number of chiral walks considered. The curves present the same convergent behavior as the AuPR, reported in Fig. 2(b), and the same considerations apply, although the variation among curves and each point of them is much smaller.

Appendix B: Dynamical distance between walker evolutions

A possible tool to determine the difference in evolution between a QW and the corresponding RW both starting from the same localized state $|j\rangle$ is the so-called quantum-classical distance [40],

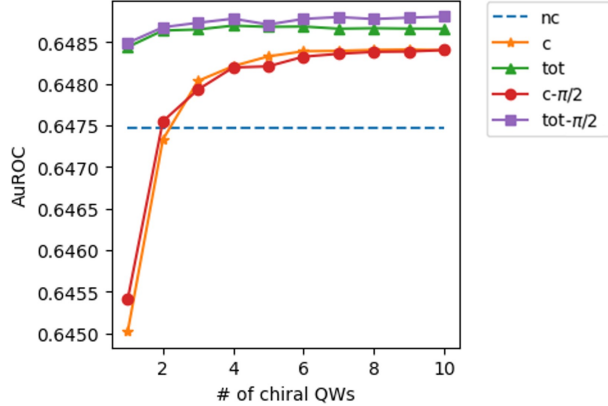


FIG. 6. Convergence of the average AuROC at 10% link removal obtained from 10-fold cross-validation on the Musculus-HINT network. Labels follow the same nomenclature as Fig. 2.

defined at time t as

$$\mathcal{D}_{QC}^j(t) = 1 - \mathcal{F}[\hat{\sigma}_j(t), \hat{\rho}_j(t)] = 1 - \sum_{k=1}^n P_{jk}^{\text{RW}}(t) P_{jk}^{\text{QW}}(t), \quad (\text{B1})$$

where $\hat{\sigma}_j$ and $\hat{\rho}_j$ are the classical and quantum density matrices at time t , respectively, and $\mathcal{F}[\hat{\sigma}_j, \hat{\rho}_j] = \text{Tr}[(\sqrt{\hat{\sigma}_j} \hat{\rho}_j \sqrt{\hat{\sigma}_j})^{1/2}]^2$ is the fidelity between states. In Eq. (B1) we used the fact that $\hat{\rho}_j$ is a pure state. A global distance, independent of the initial state $|j\rangle$, can be defined as $\mathcal{D}_{QC}(t) = \max\{\mathcal{D}_{QC}^j(t)\}$. In all the cases we considered in this paper, this distance, when evaluated between each walker and the corresponding RW, is extremely high ($\mathcal{D}_{QC} > 0.99$). Additionally, we show in Fig. 7(a) the distributions of this distance for two swarms evolving with $t = 1$ on the Musculus-HINT network at 10% link removal. Each swarm was built with one of the two sampling methods described in Sec. III A 1, that is, either with random phases in the whole continuous interval $[-\pi, \pi]$ or with multiples of $\pi/2$. As we see, the only case which distinguishes itself in both distributions is the nc-QW, which does not possess any directional bias and thus behaves slightly differently with respect to the other c-QW's. That said, the two distributions are mostly overlapping, showing very similar averages and standard deviation. This suggests that this quantity alone does not provide us with any useful insights into the different behaviors of different sampling methods.

Consequently, we generalize Eq. (B1) to the definition of a distance between the evolution of any two QW's, either chiral or non-chiral, evolving on the same network. Considering, as before, the case in which the two walkers l and m start from the same localized state $|j\rangle$:

$$\mathcal{D}_{lm}^j(t) = 1 - \mathcal{F}[\hat{\rho}_{j,l}(t), \hat{\rho}_{j,m}(t)] = 1 - |\langle \psi_{j,l}(t) | \psi_{j,m}(t) \rangle|^2 = 1 - |\langle j | \mathcal{U}_l^\dagger(t) \mathcal{U}_m(t) | j \rangle|^2, \quad (\text{B2})$$

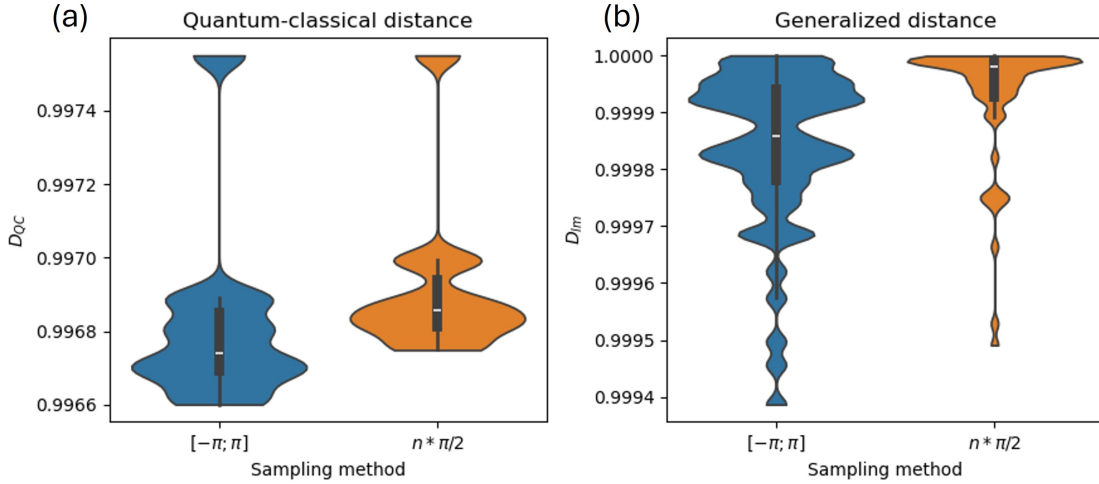


FIG. 7. Violin plots showing the distribution of (a) the quantum-classical distance \mathcal{D}_{QC} between a QW and the corresponding RW and (b) the generalized distance \mathcal{D}_{lm} between pairs (l, m) of QW's, both as described in the text and maximized on all possible starting nodes $|j\rangle$. Two swarms built with different sampling methods were considered, both made up of 10 c-QW's and the corresponding nc-QW. The first sampling methods (blue) considered phases in the continuous interval $[-\pi, \pi]$; the second (orange) considered only multiples of $\pi/2$.

where we used the fact that both states are pure. Its global equivalent on the set of all possible localized initial states is $\mathcal{D}_{lm}(t) = \max\{\mathcal{D}_{lm}^j(t)\}$.

Figure 7(b) shows the distributions of the quantity $\mathcal{D}_{lm}(t = 1)$ for the same cases as in Fig. 7(a). In this case, there is no appreciable difference in either considering the distance between a c-QW and the nc-QW, or between two c-QW's. However, now the two distributions are noticeably different, with the $\pi/2$ -method showing a much more squeezed distribution around 1, which is the maximum possible value of the distance. This shows that, while still showing similar distances with respect to the RW evolution, the $\pi/2$ method produces a set of evolutions that are as different as possible, thus exploring the possible configurational space in a much more efficient manner with respect to the $[-\pi, \pi]$ -method.

-
- [1] Lada A. Adamic and Eytan Adar. Friends and neighbors on the web. *Social Networks*, 25(3):211–230, 2003.
- [2] Nur Nasuha Daud, Siti Hafizah Ab Hamid, Muntadher Saadoon, Firdaus Sahran, and Nor Badrul Anuar. Applications of link prediction in social networks: A review. *Journal of Network and Computer Applications*, 166:102716, 2020.

- [3] Anisha Kumari, Ranjan Kumar Behera, Kshira Sagar Sahoo, Anand Nayyar, Ashish Kumar Luhach, and Satya Prakash Sahoo. Supervised link prediction using structured-based feature extraction in social network. *Concurrency and Computation: Practice and Experience*, 34(13):e5839, 2022.
- [4] István A. Kovács, Katja Luck, Kerstin Spirohn, Yang Wang, Carl Pollis, Sadie Schlabach, Wenting Bian, Dae-Kyum Kim, Nishka Kishore, Tong Hao, Michael A. Calderwood, Marc Vidal, and Albert-László Barabási. Network-based prediction of protein interactions. *Nature Communications*, 10(1):1240, Mar 2019.
- [5] Khushnood Abbas, Alireza Abbasi, Shi Dong, Ling Niu, Laihang Yu, Bolun Chen, Shi-Min Cai, and Qambar Hasan. Application of network link prediction in drug discovery. *BMC Bioinformatics*, 22(1):187, Apr 2021.
- [6] Ho Yin Yuen and Jesper Jansson. Normalized l3-based link prediction in protein–protein interaction networks. *BMC Bioinformatics*, 24(1):59, Feb 2023.
- [7] Ahmad F. Al Musawi, Satyaki Roy, and Preetam Ghosh. A review of link prediction applications in network biology. *IEEE Access*, 13:54997–55016, 2025.
- [8] Renu Goel, HC Harsha, Akhilesh Pandey, and TS Keshava Prasad. Human protein reference database and human proteinpedia as resources for phosphoproteome analysis. *Molecular BioSystems*, 8(2):453–463, 2012.
- [9] Jishnu Das and Haiyuan Yu. Hint: High-quality protein interactomes and their applications in understanding human disease. *BMC Systems Biology*, 6(1):92, Jul 2012.
- [10] Diego Alonso-López, Francisco J Campos-Laborie, Miguel A Gutiérrez, Luke Lambourne, Michael A Calderwood, Marc Vidal, and Javier De Las Rivas. Apid database: redefining protein–protein interaction experimental evidences and binary interactomes. *Database*, 2019:baz005, 01 2019.
- [11] Katja Luck, Dae-Kyum Kim, Luke Lambourne, Kerstin Spirohn, Bridget E. Begg, Wenting Bian, Ruth Brignall, Tiziana Cafarelli, Francisco J. Campos-Laborie, Benoit Charloteaux, Dongsic Choi, Atina G. Coté, Meaghan Daley, Steven Deimling, Alice Desbuleux, Amélie Dricot, Marinella Gebbia, Madeleine F. Hardy, Nishka Kishore, Jennifer J. Knapp, István A. Kovács, Irma Lemmens, Miles W. Mee, Joseph C. Mellor, Carl Pollis, Carles Pons, Aaron D. Richardson, Sadie Schlabach, Bridget Teeking, Anupama Yadav, Mariana Babor, Dawit Balcha, Omer Basha, Christian Bowman-Colin, Suet-Feung Chin, Soon Gang Choi, Claudia Colabella, Georges Coppin, Cassandra D’Amata, David De Ridder, Steffi De Rouck, Miquel Duran-Frigola, Hanane Ennajdaoui, Florian Goebels, Liana Goehring, Anjali Gopal, Ghazal Haddad, Elodie Hatchi, Mohamed Helmy, Yves Jacob, Yoseph Kassa, Serena Landini, Roujia Li, Natascha van Lieshout, Andrew MacWilliams, Dylan Markey, Joseph N. Paulson, Sudharshan Rangarajan, John Rasla, Ashyad Rayhan, Thomas Rolland, Adriana San-Miguel, Yun Shen, Dayag Sheykhkarimli, Gloria M. Sheynkman, Eyal Simonovsky, Murat Taşan, Alexander Tejada, Vincent Tropepe, Jean-Claude Twizere, Yang Wang, Robert J. Weatheritt, Jochen Weile, Yu Xia, Xinping Yang, Esti Yeger-Lotem, Quan Zhong, Patrick Aloy, Gary D. Bader, Javier De Las Rivas, Suzanne Gaudet, Tong Hao, Janusz Rak, Jan Tavernier, David E. Hill, Marc Vidal, Frederick P.

- Roth, and Michael A. Calderwood. A reference map of the human binary protein interactome. *Nature*, 580(7803):402–408, Apr 2020.
- [12] Rose Oughtred, Jennifer Rust, Christie Chang, Bobby-Joe Breitkreutz, Chris Stark, Andrew Willems, Lorrie Boucher, Genie Leung, Nadine Kolas, Frederick Zhang, Sonam Dolma, Jasmin Coulombe-Huntington, Andrew Chatr-aryamontri, Kara Dolinski, and Mike Tyers. The biogrid database: A comprehensive biomedical resource of curated protein, genetic, and chemical interactions. *Protein Science*, 30(1):187–200, 2021.
- [13] Alicia L Richards, Manon Eckhardt, and Nevan J Krogan. Mass spectrometry-based protein–protein interaction networks for the study of human diseases. *Molecular Systems Biology*, 17(1):e8792, 2021.
- [14] Steven Wang, Runxin Wu, Jiaqi Lu, Yijia Jiang, Tao Huang, and Yu-Dong Cai. Protein-protein interaction networks as miners of biological discovery. *PROTEOMICS*, 22(15-16):2100190, 2022.
- [15] Vinay Kumar and Kunal Roy. Chapter twelve - protein-protein interaction network analysis for the identification of novel multi-target inhibitors and target mirnas against alzheimer’s disease. In Vijay Kumar Prajapati, editor, *Translational Bioinformatics*, volume 139 of *Advances in Protein Chemistry and Structural Biology*, pages 405–467. Academic Press, 2024.
- [16] Joseph Loscalzo. Molecular interaction networks and drug development: Novel approach to drug target identification and drug repositioning. *The FASEB Journal*, 37(1):e22660, 2023. e22660 202201683R.
- [17] Jia-Xin Liu, Xiao Zhang, Yuan-Qin Huang, Ge-Fei Hao, and Guang-Fu Yang. Multi-level bioinformatics resources support drug target discovery of protein–protein interactions. *Drug Discovery Today*, 29(5):103979, 2024.
- [18] Cristina Camps-Fajol, Debora Cavero, Jordi Minguillón, and Jordi Surrallés. Targeting protein-protein interactions in drug discovery: Modulators approved or in clinical trials for cancer treatment. *Pharmacological Research*, 211:107544, 2025.
- [19] Georgios N. Dimitrakopoulos, Maria I. Klapa, and Nicholas K. Moschonas. How far are we from the completion of the human protein interactome reconstruction? *Biomolecules*, 12(1), 2022.
- [20] Kayra Kosoglu, Zeynep Aydin, Nurcan Tuncbag, Attila Gursoy, and Ozlem Keskin. Structural coverage of the human interactome. *Briefings in Bioinformatics*, 25(1):bbad496, 01 2024.
- [21] Elahe Nasiri, Kamal Berahmand, Mehrdad Rostami, and Mohammad Dabiri. A novel link prediction algorithm for protein-protein interaction networks by attributed graph embedding. *Computers in Biology and Medicine*, 137:104772, 2021.
- [22] Kanchan Jha, Sriparna Saha, and Hiteshi Singh. Prediction of protein–protein interaction using graph neural networks. *Scientific Reports*, 12(1):8360, May 2022.
- [23] Jun Hu, Zhe Li, Bing Rao, Maha A. Thafar, and Muhammad Arif. Improving protein-protein interaction prediction using protein language model and protein network features. *Analytical Biochemistry*, 693:115550, 2024.
- [24] Weiping Liu and Linyuan Lü. Link prediction based on local random walk. *Europhysics Letters*, 89(5):58007, 2010.

- [25] Manuel Curado. Return random walks for link prediction. *Information Sciences*, 510:99–107, 2020.
- [26] Feng Xia, Jiaying Liu, Hansong Nie, Yonghao Fu, Liangtian Wan, and Xiangjie Kong. Random walks: A review of algorithms and applications. *IEEE Transactions on Emerging Topics in Computational Intelligence*, 4(2):95–107, 2020.
- [27] Adilson Vital Jr, Filipi Nascimento Silva, and Diego Raphael Amancio. Comparing random walks in graph embedding and link prediction. *PLoS one*, 19(11):e0312863, 2024.
- [28] Wen Liang, Fei Yan, Abdullah M. Ilyasu, Ahmed S. Salama, and Kaoru Hirota. A simplified quantum walk model for predicting missing links of complex networks. *Entropy*, 24(11), 2022.
- [29] Mark Goldsmith, Harto Saarinen, Guillermo García-Pérez, Joonas Malmi, Matteo A. C. Rossi, and Sabrina Maniscalco. Link prediction with continuous-time classical and quantum walks. *Entropy*, 25(5), 2023.
- [30] João P. Moutinho, André Melo, Bruno Coutinho, István A. Kovács, and Yasser Omar. Quantum link prediction in complex networks. *Phys. Rev. A*, 107:032605, Mar 2023.
- [31] Y. Aharonov, L. Davidovich, and N. Zagury. Quantum random walks. *Phys. Rev. A*, 48:1687–1690, Aug 1993.
- [32] Oliver Mülken and Alexander Blumen. Continuous-time quantum walks: Models for coherent transport on complex networks. *Physics Reports*, 502(2):37–87, 2011.
- [33] Kunkun Wang, Yuhao Shi, Lei Xiao, Jingbo Wang, Yogesh N. Joglekar, and Peng Xue. Experimental realization of continuous-time quantum walks on directed graphs and their application in pagerank. *Optica*, 7(11):1524–1530, Nov 2020.
- [34] Karuna Kadian, Sunita Garhwal, and Ajay Kumar. Quantum walk and its application domains: A systematic review. *Computer Science Review*, 41:100419, 2021.
- [35] Xiaogang Qiang, Shixin Ma, and Haijing Song. Quantum walk computing: Theory, implementation, and application. *Intelligent Computing*, 3:0097, 2024.
- [36] Harto Saarinen, Mark Goldsmith, Rui-Sheng Wang, Joseph Loscalzo, and Sabrina Maniscalco. Disease gene prioritization with quantum walks. *Bioinformatics*, 40(8):btac513, 08 2024.
- [37] Viacheslav Dubovitskii, Aritra Bose, Filippo Utro, and Laxmi Pardia. On quantum random walks in biomolecular networks, 2025.
- [38] Dawei Lu, Jacob D. Biamonte, Jun Li, Hang Li, Tomi H. Johnson, Ville Bergholm, Mauro Faccin, Zoltán Zimborás, Raymond Laflamme, Jonathan Baugh, and Seth Lloyd. Chiral quantum walks. *Phys. Rev. A*, 93:042302, Apr 2016.
- [39] Massimo Frigerio, Claudia Benedetti, Stefano Olivares, and Matteo G. A. Paris. Generalized quantum-classical correspondence for random walks on graphs. *Phys. Rev. A*, 104:L030201, Sep 2021.
- [40] Massimo Frigerio, Claudia Benedetti, Stefano Olivares, and Matteo G. A. Paris. Quantum-classical distance as a tool to design optimal chiral quantum walks. *Phys. Rev. A*, 105:032425, Mar 2022.
- [41] Simon Apers, Shantanav Chakraborty, Leonardo Novo, and Jérémie Roland. Quadratic speedup for spatial search by continuous-time quantum walk. *Phys. Rev. Lett.*, 129:160502, Oct 2022.

- [42] Simone Cavazzoni, Luca Razzoli, Paolo Bordone, and Matteo G. A. Paris. Perturbed graphs achieve unit transport efficiency without environmental noise. *Phys. Rev. E*, 106:024118, Aug 2022.
- [43] Massimo Frigerio and Matteo G.A. Paris. Swift chiral quantum walks. *Linear Algebra and its Applications*, 673:28–45, 2023.
- [44] Emilio Annoni, Massimo Frigerio, and Matteo G. A. Paris. Enhanced quantum transport in chiral quantum walks. *Quantum Information Processing*, 23(4):117, Mar 2024.
- [45] Sara Finocchiaro, Giovanni O. Luilli, Giuliano Benenti, Matteo G. A. Paris, and Luca Razzoli. Optimal quantum transport on a ring via locally monitored chiral quantum walks. *Phys. Rev. E*, in press, 2025.
- [46] A Khaliq, A Sett, J B Wang, and J Twamley. Controlled information transfer in continuous-time chiral quantum walks. *New Journal of Physics*, 23(8):083005, aug 2021.
- [47] Alberto Bottarelli, Massimo Frigerio, and Matteo G. A. Paris. Quantum routing of information using chiral quantum walks. *AVS Quantum Science*, 5(2):025001, 04 2023.
- [48] Giovanni Ragazzi, Simone Cavazzoni, Claudia Benedetti, Paolo Bordone, and Matteo G. A. Paris. Scalable structure for chiral quantum routing. *Entropy*, 27(5), 2025.
- [49] Simone Cavazzoni, Giovanni Ragazzi, Paolo Bordone, and Matteo G. A. Paris. Perfect chiral quantum routing. *Phys. Rev. A*, 111:032439, Mar 2025.
- [50] Octavi Boada, Leonardo Novo, Fabio Sciarrino, and Yasser Omar. Quantum walks in synthetic gauge fields with three-dimensional integrated photonics. *Phys. Rev. A*, 95:013830, Jan 2017.
- [51] C. Cedzich, T. Geib, A. H. Werner, and R. F. Werner. Quantum walks in external gauge fields. *Journal of Mathematical Physics*, 60(1):012107, 01 2019.
- [52] Luca Razzoli, Luca Ghirardi, Ilaria Siloi, Paolo Bordone, and Matteo G. A. Paris. Lattice quantum magnetometry. *Phys. Rev. A*, 99:062330, Jun 2019.
- [53] Tao Zhou. Progresses and challenges in link prediction. *iScience*, 24(11), Nov 2021.
- [54] Takaya Saito and Marc Rehmsmeier. The precision-recall plot is more informative than the roc plot when evaluating binary classifiers on imbalanced datasets. *PloS one*, 10(3):e0118432, 2015.
- [55] Chris Stark, Bobby-Joe Breitkreutz, Teresa Reguly, Lorrie Boucher, Ashton Breitkreutz, and Mike Tyers. Biogrid: a general repository for interaction datasets. *Nucleic Acids Research*, 34(suppl_1):D535–D539, 01 2006.
- [56] TS Keshava Prasad, Renu Goel, Kumaran Kandasamy, Shivakumar Keerthikumar, Sameer Kumar, Suresh Mathivanan, Deepthi Telikicherla, Rajesh Raju, Beema Shafreen, Abhilash Venugopal, et al. Human protein reference database—2009 update. *Nucleic acids research*, 37(suppl_1):D767–D772, 2009.
- [57] M. E. J. Newman. Clustering and preferential attachment in growing networks. *Phys. Rev. E*, 64:025102, Jul 2001.
- [58] Lin Yao, Luning Wang, Lv Pan, and Kai Yao. Link prediction based on common-neighbors for dynamic social network. *Procedia Computer Science*, 83:82–89, 2016. The 7th International Conference on Ambient Systems, Networks and Technologies (ANT 2016) / The 6th International Conference on Sustainable Energy Information Technology (SEIT-2016) / Affiliated Workshops.

- [59] Linyuan Lü, Liming Pan, Tao Zhou, Yi-Cheng Zhang, and H. Eugene Stanley. Toward link predictability of complex networks. *Proceedings of the National Academy of Sciences*, 112(8):2325–2330, 2015.